Int J Adv Manuf Technol (2013) 69:31–39
DOI 10.1007/s00170-013-5003-0

ORIGINAL ARTICLE

Studies on wears of ultrafine-grained ceramic tool and common ceramic tool during hard turning using Archard wear model

H-J Hu · W-J Huang

Received: 26 November 2012 / Accepted: 8 April 2013 / Published online: 21 April 2013

Abstract Hardened steels are difficult to be machined due to their high tensile strength and work-hardening rate, low thermal conductivity, and abrasive behavior. In this paper, finite element modeling (FEM) approaches with lagrangian increment method for 3D metal turning of hardened steel H13 by common ceramic tool and ultrafine-grained tool respectively have been investigated by simulation of DEFORM-3D software and turning test. Conditions of initial and boundary and turning process parameters have been chosen. Material properties of H13 and ceramic have been described in details. Johnson–Cook model of H13 model has been applied to the hard turning modeling. Archard wear model has been built, and the correlation coefficients were decided by reciprocating friction experiments. The simulation results showed that predicted primary turning force and maximum temperature in common ceramic are bigger than which was caused by ultrafine-grained ceramic tool for the ultrafine-grained ceramic tools have better thermal stability and bigger hardness. The wear depths of common ceramic tool are about many times than that of ultrafine-grained ceramic tool according to the simulation and experimental results. And their wear patterns are very different. The FEM simulation results have entirely explicated experimental results. The obtained results would provide the fundamental and practical guidelines of tool material choice for hard turning.

Keywords Ultrafine-grained ceramic · Finite element method · Hard turning · Flank wear

H.-J. Hu (✉) · W.-J. Huang (✉)
College of Material Science and Engineering, Chongqing University of Technology, Chongqing 400050, China
e-mail: hhj@cqut.edu.cn
e-mail: huangweijiu@cqut.edu.cn

1 Introduction

Hardened steel is often used for medium or high carbon steels which have been quenched followed by tempering. The quenching results in the formation of martensite, and the fraction of which is reduced to the desired amount during tempering [1–3]. The martensite is the most common state for many steel products. But the same steel composition in annealed state will be softer and can be machined easily [4]. AISI H13 die steel possesses good resistance to heat checking, high strength and high toughness. So, H13 steel has been applied widely to produce many kinds of hot work dies [5]. Hard turning is the process of turning hardened pieces with hardness between 58 and 62 HRC. The intermediate heat treatment can be eliminated with hard turning [6,7]. Hard turning could reduce and even eliminate some finish grinding and improve the machined surface and replace grinding for finishing various components of hardened steels, such as transmission shafts, bearings, and gears and other important parts. But the cutter tool is exposed to a very severe environment with very high stress and temperature during hard turning. For a tool to perform successfully under these severe conditions and to have a good surface quality, the tool material has to be carefully selected [8].

Wears would result in the failures of the turning cutter if the tool wear reach certain extent; the tool or edge change has to be replaced to guarantee the ordinary turning action. Under high temperature and pressure and sliding velocity and mechanical or thermal shock in turning area, cutter has normally complex wear appearance, which consists of some basic wear types such as crater wear, flank wear, fatigue crack, insert breakage, thermal crack, brittle crack, plastic deformation, and build-up edge, etc. [9].

There are many applications of turning tool-coated micron-sized Al_2O_3, but the studies on nano-Al_2O_3 tool

are very limited by simulation ways. Finite element modeling (FEM) analysis is a useful investigative way of intensive studies for the metal turning process. Many papers have introduced on FEM of the metal turning process. In this paper, we used simulation results to explicate the differences of wear mechanism for ultrafine-grained ceramic and common ceramic tool. This research could design fundamental and practical guidelines of the hard turning about the choice of ceramic tool.

It is very difficult to acquire the data by studying the temperature and force and wear of tool during turning experiments. Many researchers applied finite element simulation technologies to study the turning process deeply, which could make the turning tool product more precise and more reliable and shorten the time for developing new turning tool. Li et al. used two-dimensional fully thermomechanical coupled finite element model to simulate machining hardened steel SKD11 component [10]. Reginaldo et al. [11] used finite element model simulations and experiments with three different coatings; the results of tool wear, cutting force, and surface finish obtained from the turning operation on hardened AISI 4340 using PCBN-coated and PCBN-uncoated edges are obtained. Lorentzon [7] applied finite element model of tool wear to predict the worn geometry quantitatively in cemented carbide tool machining nickel-based alloys. In this study, the 3D finite element model is used to understand the fundamentals of hard turning process and predict the flank wears for ultrafine-grained ceramic tool and common ceramic tool. Simulation and experimental works have investigated the influences of tools with different dimension grains on tool flank wear in hard turning of H13 cold work tool steel.

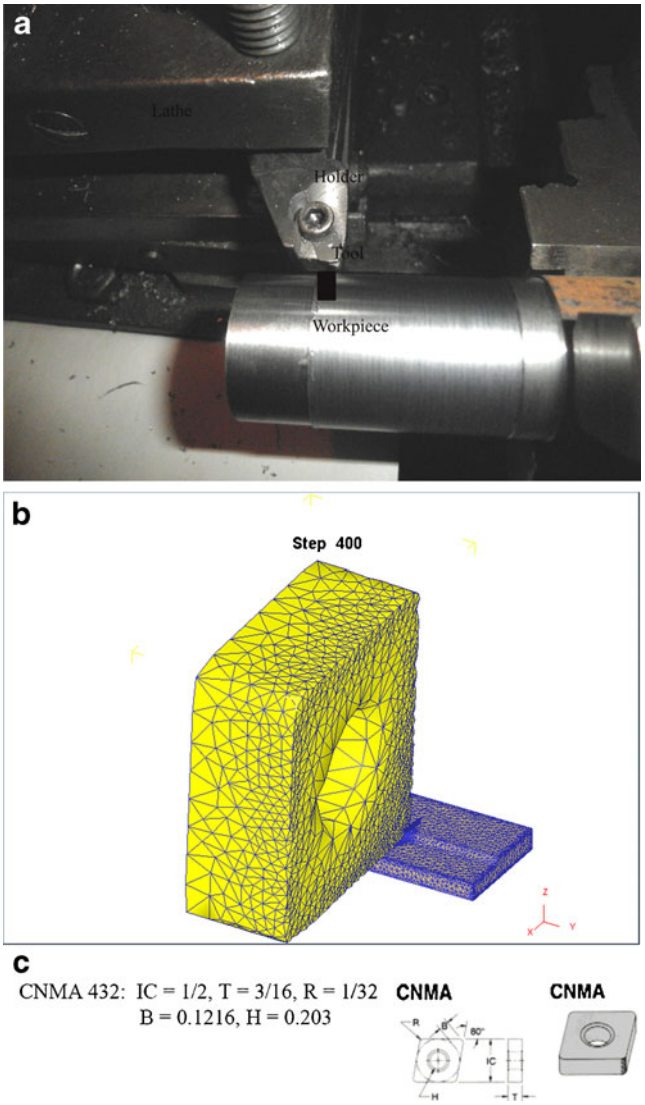

Fig. 1 Experimental setup of H13 hard turning (**a**). Finite element method model of tool workpiece for the FEM simulations after a tool stroke of 4 mm (**b**). The CNMA tool geometry (**c**)

2 Mathematical models for hard turning

The DEFORM-3D software can be used to simulate the turning process. These modeling procedures enable the engineers to study the process evolution for any change in process conditions [7]. Cutting forces, cutting temperatures, chip shape, tool wears, and tool life can be calculated using the manufacturing module in this software. In this paper, a commercial software code DEFORM-3D v6.0 and a lagrangian modeling approach have been used to conduct the 3D FEM simulation of orthogonal cutting and ultrafine-grained ceramic and common ceramic tool with different grains dimension have been considered.

2.1 Finite element models

For hard turning the rotating workpiece, tool and holder and lathe and their install relationship are shown in Fig. 1a, and the analysis domain in workpiece are marked with a black color. The material is attached to the mesh [12]. Automatic end adaptive remeshing has been taken into account the severe distortion of mesh elements near the tool tip, so very fine meshes have been form near the tool tip in the deformation zone of the workpiece and the edge of the 3D model tool as shown illustratively in Fig. 1b. Four-node elements in both workpiece and tool models were used for the deformations occurring during the hard turning process. The turning tool was meshed by using rigid elements. The turning tool was set to move in Y direction. Figure 1b shows the finite element model of tool-workpiece for the simulations after stroke of 4 mm. The workpiece dimensions are 6.8 mm in width and 8 mm in length and 2 mm in height. The workpiece was considered as a plastic object, initially meshed with 40,670 elements, and the tool was a rigid object meshed with more than 11,506 elements. The

CNMA tool geometry shown in Fig. 1c was selected from the insert library of the DEFORM software. Once the insert is identified, the basic parameters of this insert can be obtained.

2.2 Material models

It is very important to establish the material models and properties data in order to get correct simulation results. Figure 2a shows the curves of thermal conductivity and heat capacity varying with temperature for H13 work materials. Young's modulus and coefficient of linear expansion for H13 varying with temperature are described in Fig. 2b, c, respectively, and the data were obtained from the material library of the DEFORM-3D software. In the DEFORM software, high-precision flow stress models are considered to be highly necessary to represent work material constitutive behavior under high-strain-rate deformation conditions. The constitutive model was established by Johnson and Cook [13]. The work material model represents plastic, elastic, and thermomechanical behavior of the material deformations satisfactorily during the machining process. Strain, strain rate, and temperature effects are individually determined as given in Eq.1. In the Johnson–Cook (J-C) model, σ is effective stress, the constant A is the initial yield strength of the material at room temperature, B, C, and m are constants, and strain rate $\dot{\bar{\varepsilon}}$ represents the plastic equivalent strain. The strain rate $\bar{\varepsilon}$ is normalized with a reference strain rate, T_{melt} is melting temperature, n is work hardening exponent, and T_{room} is room temperature.

$$\bar{\sigma} = [A + B(\bar{\varepsilon})^n \left[1 + C \ln\left(\frac{\dot{\bar{\varepsilon}}}{\dot{\bar{\varepsilon}}_0}\right)\right] \left[1 - \left(\frac{T - T_{\text{room}}}{T_{\text{melt}} - T_{\text{room}}}\right)^m\right] \tag{1}$$

The mechanical and physical properties of the ultrafine-grained ceramic and common ceramic tool material properties such as elastic modulus (E), Passion's ratio (μ), etc., of the ultrafine-grained Al_2O_3 ceramic tool are considered independent of temperature and are listed in Table 1.

2.3 Archard wear models established by experiments

There are many reasons of influences on tool wear during the actual turning process, especially the workpiece material is not homogeneous. The turning heat and temperature rise have a great influence on the turning performance. High temperatures in turning are the cause of unsatisfactory tool life. The main factor for decrease of tool wear is tool temperature dropping. Turning speed is the other main factors for tool life. The wear rate has been calculated using Archard empirical wear model in Eq.2 for every node of the tool in contact with the base material in this paper [14–16]. The main advantage of this model is that mild and slight wear can be calculated in a rather easy way, and the calculations are based on Archard's wear model, a model using contact mechanics to describe the wear behavior. The Archard wear equation is a simple model used to describe sliding wear and is based around the theory of asperity contact. The volume of the removed from tool due to

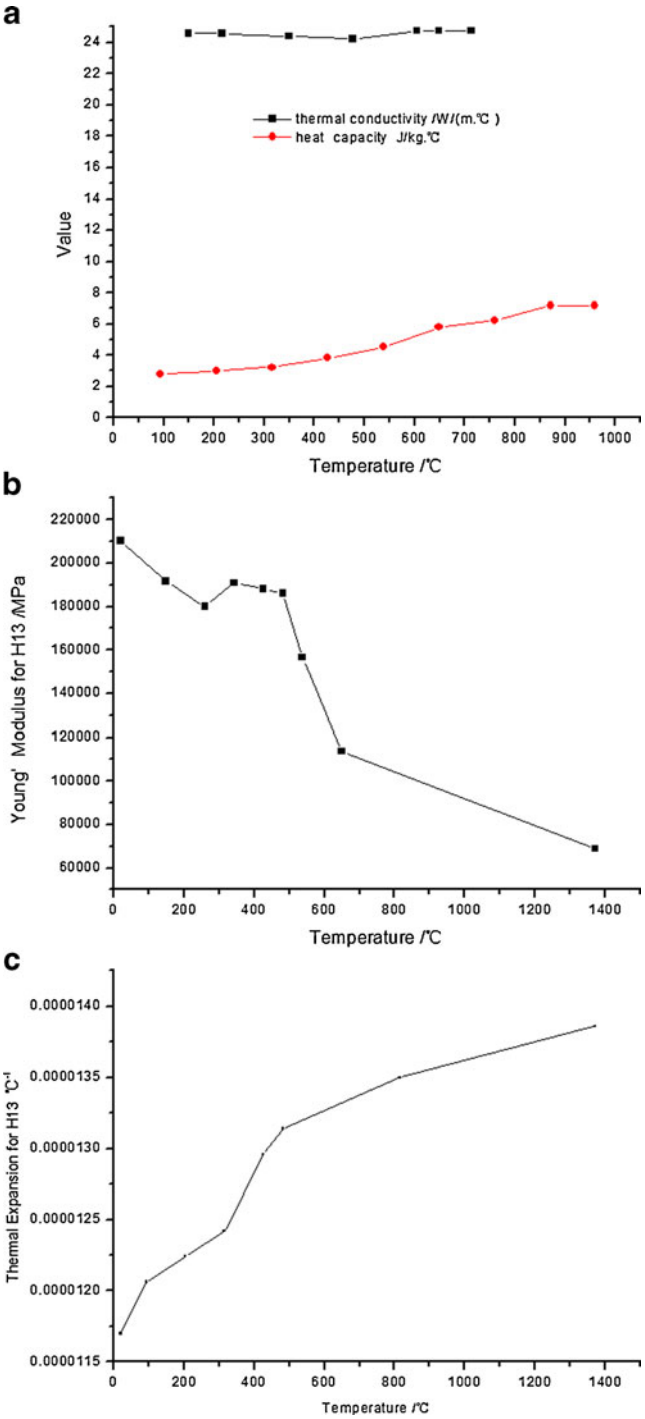

Fig. 2 Materials properties of H13, thermal conductivity and heat capacity (**a**), Young's modulus, (**b**) and coefficient of linear expansion (**c**)

Table 1 Properties of the submicron Al2O3 and common ceramic tool materials

	Common ceramic	Ultrafine-grained ceramic
Density (kg/m^3)	3,400	3,500
Young's modulus (GPa)	300	415
Poisson's ratio	0.28	0.22
Thermal expansion	3.2e−06	8.4e−06
Specific heat (J kg^{-1} K^{-1})	620	334
Thermal conductivity (W m^{-1} K^{-1})	23	7.5

wear is proportional to the work done by friction forces. The archard wear equation is a simple model used to describe sliding wear and is based on the theory of asperity contact. The influence of the temperature distribution on the material hardness is not taken into account when archard law is used and the pressure and velocity distribution often affect the predicted wear profiles more than the hardness (temperature) distribution.

$$W = \int K \frac{p^a v^b}{H^c} \mathrm{d}t \tag{2}$$

Where W is flank wear land width, p stranded for normal stress between tool flank face and workpiece, v sliding velocity, H hardness of the cutting tool material, dt time increment, and a, b, and c are experimentally calibrated coefficients and equal to 1 and 1and 2 respectively in this paper. K is therefore a measure of the severity of wear. The K value is divided by reciprocating friction experiments, the K is 5e−9 when the turning tools are made of ultrafine-grained ceramic with grain size 0.27 μm and hardness 19,000 MPa, equal to 4e−7 if the tool material is common ceramic with grain size 1.6 μm and hardness 17,300 MPa, and dt is time increment.

2.4 Simulation conditions

Heat conduction of turning is depicted by partial differential energy equation in rectangular coordinate system. The mathematical models of temperature based on the FEM can predict the temperature distributions. The turning temperature is initialized by T_0 20 °C, and the initial environmental temperature is 20 °C. Between the two contact surfaces of tool/chip, heat is conducted from the highest to the lowest temperature according to the thermal coefficient. The heat flux is given by formula (3) [17,18], and thermal transfer is considered mainly as one of important boundary conditions.

$$-\lambda(T)\frac{\partial T}{\partial y} = h(T)(T_\mathrm{s} - T_\mathrm{f}) \tag{3}$$

Where λ (T) is the thermal conductivity functions which vary with temperature, $\partial T/\partial y$ is temperature gradient along Y direction, h (T) the heat-transfer coefficient of the workpiece material and considered to be constant here, T_s the surface temperature of workpiece, and T_f the temperature of tool tip.

Interfacial friction characteristics on the cutter/chip and cutter /workpiece should be employed to account for additional heat generation and stress developments due to friction. Contact boundary conditions have been applied to nodes of workpiece and specify contact between those nodes and the surface of tool .The Newton–Raphson methods have been recommended for most problems because it generally converge in less iteration than the other available methods [19]. However, solutions are more likely to fail to converge with this method than the other methods. To represent the friction behavior by using the shear stress and the contact pressure, the generalized Coulomb's law has been used. The frictions between the workpiece/tool interfaces are considered as shear type. It is well known that this law state proportionality between shear yield stress and the contact pressure due to presence of the friction. Specifically in the DEFORM code, this relation is verified by means of von Mises yield criterion corrected to the simple shear condition and given by Eq. [20] (4).

$$\tau = \mu\sigma \Big/ \sqrt{3} \tag{4}$$

Where τ is the frictional shear stress, σ the effective flow stress of the workpiece, and μ ($0 \le \mu \le 1$) the friction factor. In the present simulations, friction factor 0.6 at the tool/chip interface has been chosen in this paper. The same value for friction factor has been assumed at the interface between the tool and workpiece. The conditions of simulation and experiments for hard metal turning are list in Table 2. The simulation conditions are identical to those of the experiments. Machining has been performed at ambient temperature, and the initial temperature of workpiece, and the tool are assumed to be equal to 20 °C.

2.5 Experimental details

The experimental setup of hard turning is illustrated in Fig. 1a. The spindle speed of the lathe can vary from 50 to 1,400 rpm continuously. The ultrafine-grained ceramic cutter and common ceramic cutter tools are used as the cutting tools, respectively. The cutting tool geometries are shown in Fig. 1c with 80° diamond shape and rake angle of 5° and clearance angle of 5°. The tool nose radius is 0.8 mm. Investigation of machining of hard AISI H13 material by cutter with different ceramic grains dimension have been carried out .The turning experiments were performed using CA6140 lathe. All experiment data have been obtained on H13 hardened steel with

Table 2 Turning conditions and tool geometry for simulations and experiments

Workpiece material	H13
Surface speed (m/min)	200
Cutting environment	Dry
Workpiece type	Plastic
Tool type	Rigid
Depth of cut (mm)	0.1
Feed rate (mm/rev)	0.1
Environment temperature (°C)	20
Convection coefficient between tools and environment (N s^{-1} mm^{-1} $°C^{-1}$)	0.02
Friction factor	0.6
Heat transfer factor (N s^{-1} mm^{-1} $°C^{-1}$)	45
Side cutting angle (deg)	−5
Back rake angle (deg)	−5
Side rake angle (deg)	5
Measured turning edge radius (mm)	17–33
Width of cut (mm)	4
Workpiece temperature (°C)	20

hardness between 60 to 65 HRC. The tool flank wear was measured by scanning electron microscope (SEM) jsm6460LV. The workpiece has been cut as 800 mm length bar with 60 mm diameter. In order to verify high-speed turning simulation results, the same turning conditions and other conditions parameters have been shown in Table 2. In this study, samples from the tip of turning tool were taken, and we cleaned and sprayed gold on the surface of the samples for microstructure observation. Microstructure observations were carried out by using SEM. The evaluation of the flank tool wear was made by a toolmaker's microscope with ×100 magnification and 100 μm scale.

3 Results and discussions

3.1 Curves of primary turning forces with ultrafine-grained ceramic tool and common ceramic tool

The high compressive and frictional contact stresses on the tool face could result in primary turning force. Usually, it is calculated just in the steady condition which makes it impossible to study the variation and cracks of cutter influenced by change of turning forces. Among machining process parameters, turning force is relatively easy to be controlled quantitatively, and connected to tool conditions directly. Abruptly increasing turning force on a tool may damage the tool or cause unexpected wears. Turning forces depend upon chip, workpiece material and turning speed, etc. Figure 3 presents the variation of the simulated turning forces along the Y directions with numerical simulation condition of high speed turning with f=0.1 mm/s and v= 200 mm/min and a very narrow range time 2.8e−5 s. The curves show that turning forces are fluctuation. At the beginning of machining the turning forces rise gradually, this is a short period and the force is increase during beginning of the tool cutting edge into a workpiece. Curves show that the predicted maximum turning force of principal directions Y are 208 N and 162 N for common ceramic tool and ultrafine-grained ceramic tool, respectively. The Y direction force for common ceramic tool is bigger than that of ultrafine-grained ceramic tool, and the former would overcome more resistance of metal along the turning direction.

3.2 Turning temperature prediction

In hard turning nearly all of energy dissipated in plastic deformation is converted into heat which raises the temperature, and temperature is the primary factor affecting the cutting tool wear. The primary heat generated in the metal turning derives from plastic deformation and friction between chip/tool interfaces. High-temperature rise would cause strength reduction of the workpiece material. High-temperature rise can induce thermal damage to the machined workpiece surface and promote oxidation of the machined surface. The oxidation layer may result in shorter service life.

At present there is no appropriate technology to measure the temperature of hard turning, and there are no simple reliable methods to measure the temperature field. Therefore, the temperature distribution is very difficult to be experimentally obtained, and temperature field analysis is obtained mostly by numerical simulations. The maximum and minimum temperature curves obtained during turning in the tool

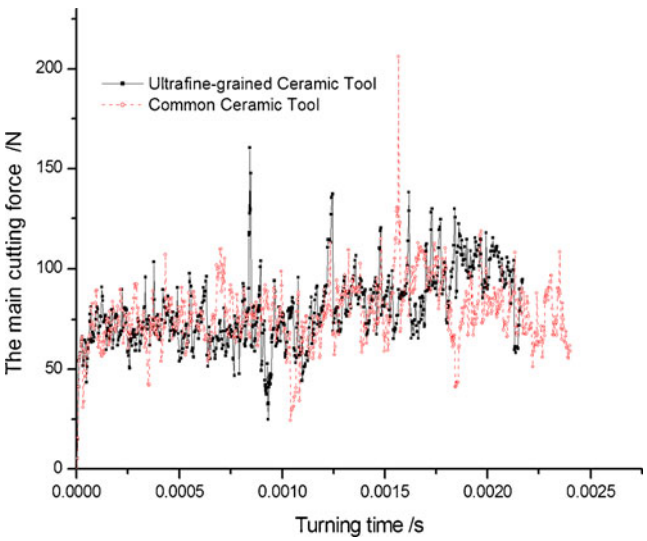

Fig. 3 Curves of primary turning force in Y directions

are shown in Fig. 4. It is established that temperatures changing with turning time till the temperature reaches steady-state during 0–0. 37 ms. As can be seen from the curves, the minimum value of the temperature for tool is about 20 °C, and the maximum for ultrafine-grained ceramic tool and common ceramic tool at 185 and 168 °C, respectively. From the trends, the tool temperature would increase with turning. Figure 5 shows the isothermal lines of machining temperature field in the tool for machining time 0.001 s. The "hot spot" temperatures around the edge at the chamfer face are between 20–118 °C for common ceramic tool and 20–105 °C for ultrafine-grained ceramic tool.

3.3 Tool wears during turning

There are many reasons of influences on tool wear during the actual turning process, especially the workpiece material is not homogeneous. In the finite element software, these effects may not be completely taken into account. Therefore, there is finite element simulation of only a qualitative discussion, that is to say, the analysis is in the normal cutting, and in the tool wear occurs relative probability as well as the tool wear trend. With this tool wear estimation program in deform software, tool wear progress under the same turning conditions as described in Table 2 is calculated.

The general relationships of wear depth versus simulation steps are shown in the Fig. 6. During the whole turning process, the total wear depths of common ceramic tool are about many times than that of ultrafine-grained ceramic tool. As turning proceeds, the amount of wears increases gradually for common ceramic tool and ultrafine-grained ceramic tool.

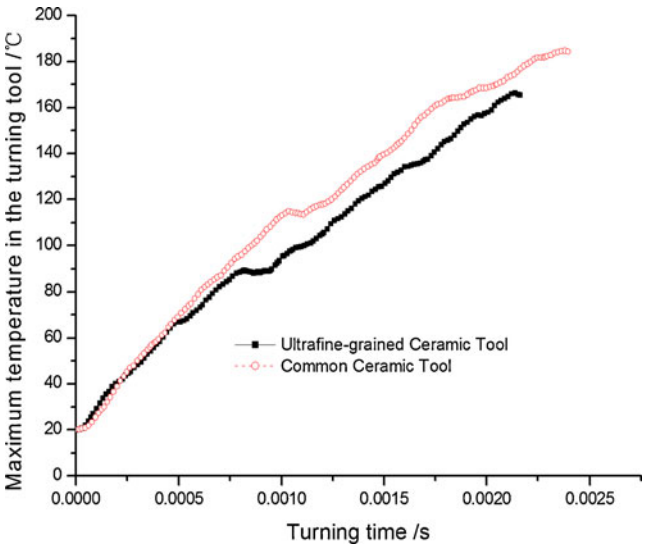

Fig. 4 Simulation maximum temperature vs. time for ultrafine-grained ceramic tool and common ceramic tool

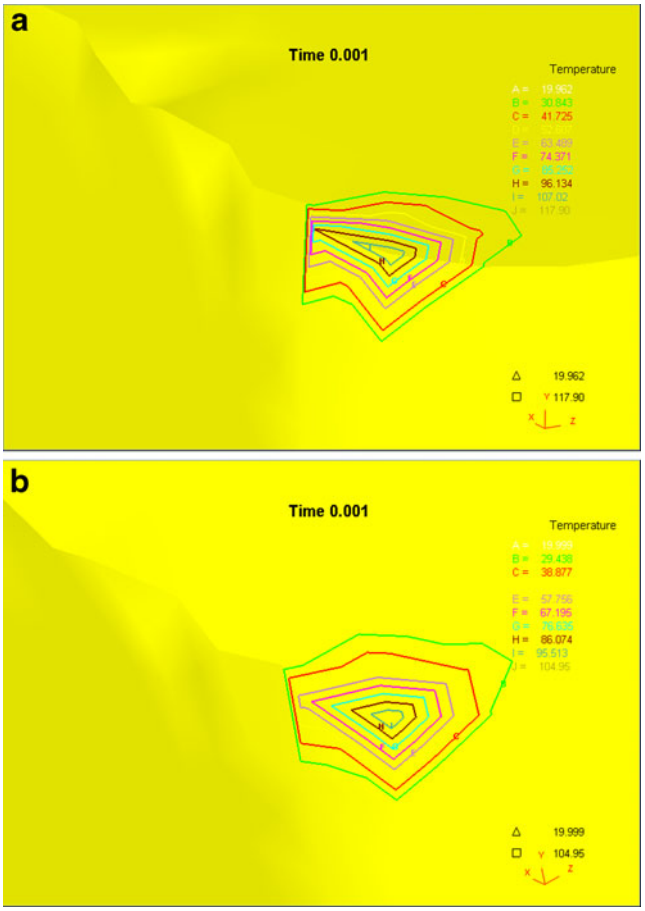

Fig. 5 The temperature distribution of machining at 0.001 s. **a** The isothermal lines of common ceramic tool. **b** For ultrafine-grained ceramic tool

In the early stage of turning, there is small wear value on common ceramic tool surface for (shown in Fig. 7a) and the maximum wear depth is 0.0000905 mm at 0.0001 s. As the cutting continues wear area increases gradually. The wear

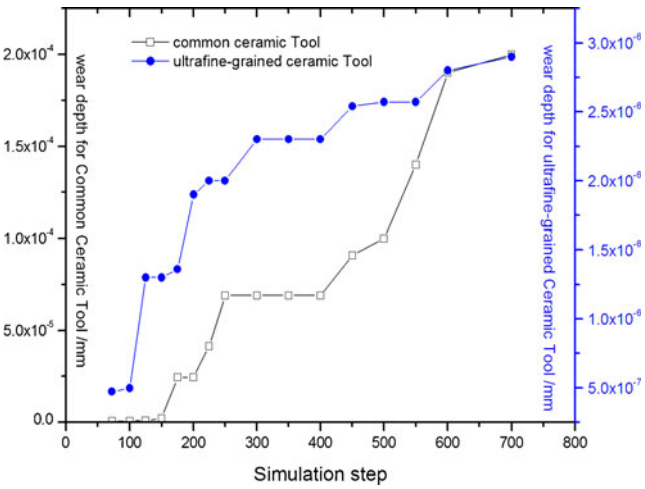

Fig. 6 Wear depths with different tool ceramic materials vary with simulation steps

has exceeded 0.000213 mm (shown in Fig. 7b) at the tip of tool when turning time is 0.0002 s. On the contrary, the wear depth is 0.0000023 and 0.00000293 mm illustrated in Fig. 7c, d, respectively. From Fig. 7c, d, it can be seen that the tool wear begin with the tip of tool, the wear spread at centre around the tip following the turning development. When the wear area increases to a certain extent, wear zone can no longer be changed too much. The wear would result in increase of cutting force and cutting temperature (shown in Fig. 4), and which would lead to the workpiece and the tool vibration, and make surface finish poor and dimension accuracy decrease. The dominating basic wear types vary with the cutting conditions, crater wear, and flank wear are the most common wear types [21,22]. It is found that the flank wears are main wear type in these simulations, flank wear is caused by the friction between the newly machined workpiece surface and the tool flank face and occurs on the flank of the tool below the cutting edge, and wear mechanism is very complex.

3.4 Microstructures for tool wears

Figure 8 shows the flank wear and micro tipping of common ceramic and ultrafine-grained ceramic tool observed with SEM after experimental tests when turning speed is 200 m/min and feed rate 0.10 mm/rev and turning length 600 mm. It is obvious that the wear depths of common ceramic tool are bigger than that of ultrafine-grained ceramic tool. The size of the flank wear can be measured as the distance between the top of the cutting edge and the bottom of the flank wear land. There are scratched marks on the tool flank. The extending directions of wear grooves are different obviously for common ceramic and ultrafine-grained ceramic tool, the former perpendicular to the blade, and the later parallel to the blade of turning tool. From Fig. 8, the values of flank wears are about 0.18 and 0.538 mm for the ultrafine-grained ceramic tool and common ceramic tool, respectively. The flank wears of tool tip presents grooves generated by abrasive mechanism and adhesion of material which could be due to the abrasive action of hard carbide particles of the work material. It is well-known the wear is related to cutting temperature during hard turning. The turning tool is subjected to high temperature and pressure near the tip of tool during hard turning. Therefore, the pressure and temperature could cause flank and crater wear as well as possible groove wear on the surface of tool tip. For good thermal stability and bigger hardness for ultrafine-grained ceramic, the wear resistance for hard turning of ultrafine-grained ceramic is super to that of common ceramic. At the tool flank/workpiece surface contact area, tool particles adhering to the workpiece surface are

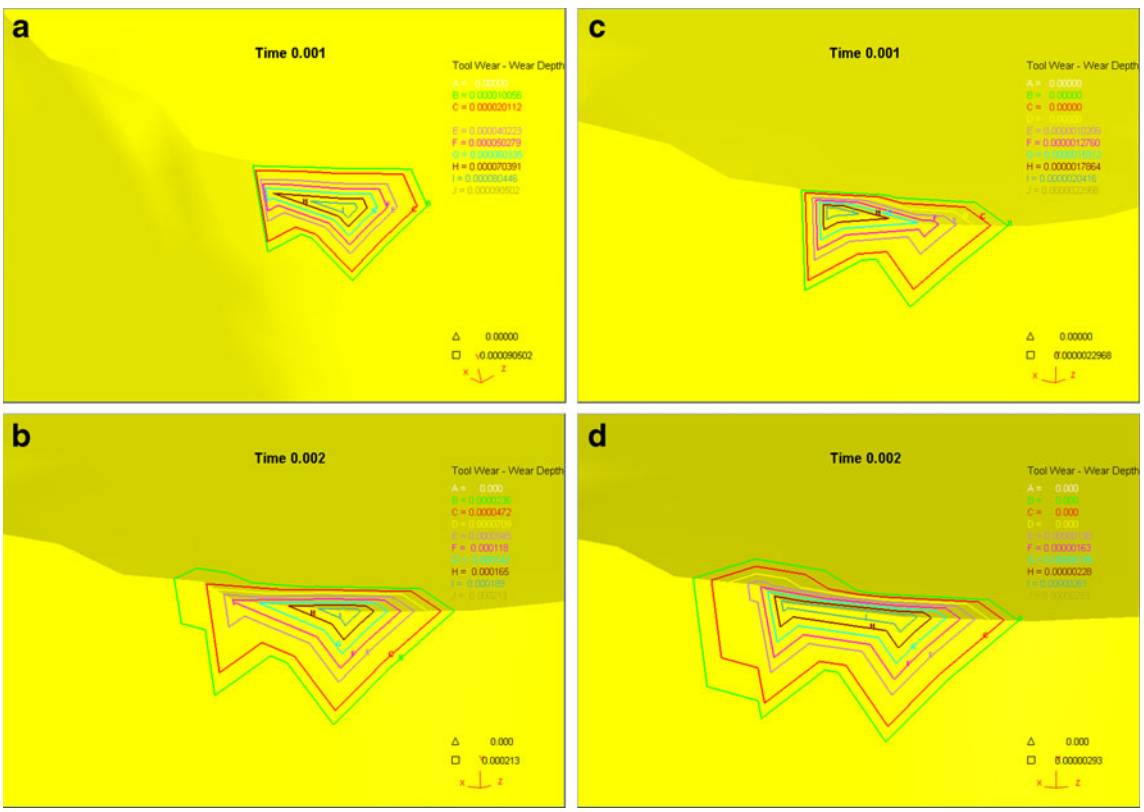

Fig. 7 Wear depth evolution with different ceramic materials tool vary with turning time: **a** turning time 0.001 s, common ceramic tool; **b** turning time 0.002 s, common ceramic tool; **c** turning time 0.001 s, ultrafine-grained ceramic tool; and **d** turning time 0.002 s, ultrafine-grained ceramic tool

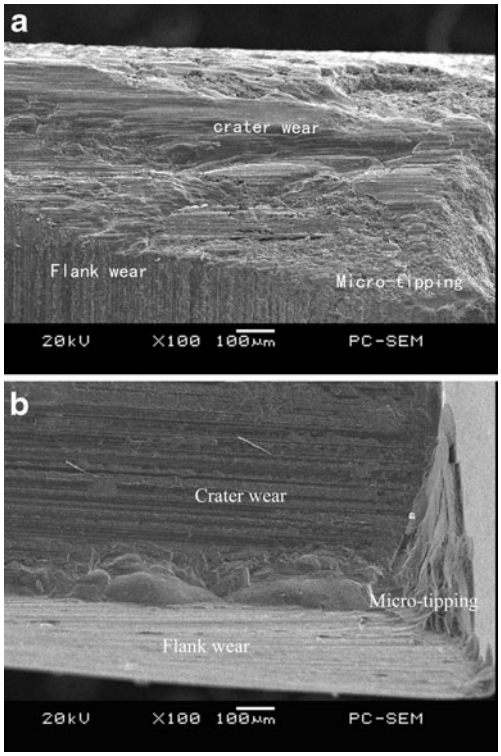

Fig. 8 SEM views of the flank and micro-tipping for the common ceramic (**a**) and ultrafine-grained ceramic tool tip (**b**; turning speed is 200 m/min feed rate (0.10 mm/rev) and turning length is 600 mm)

periodically taken off. Adhesion of the tool and workpiece increases at higher temperatures. Adhesive wear occurs if some hard inclusions or particles escaped from tool. It should give rise to concern when the rate of flank wear becomes too large [9,23].

4 Conclusions

The FEM simulations and experimental studies of turning of alloys steel AISI H13 by common and ultrafine-grained ceramic tool were studied in the in this paper. The following conclusions can be drawn:

(1) Coupled thermo-mechanical 3D FEM models of hard turning incorporating the material properties and simulation conditions (initial and boundary) have been founded, four-node elements in both workpiece and tool models have been meshed. Thermal conductivity and heat capacity and Young's modulus and coefficient of linear expansion for H13 work materials have been introduced. A detailed friction modeling at the interfaces have been carried out. Archard wear model has been built and the coefficients were decided by reciprocating friction experiments.

(2) Solution techniques are performed to predict cutting forces, temperatures, and tool wear distributions and turning forces are fluctuation. The predicted primary turning force and maximum temperature in common ceramic is the bigger than which caused by ultrafine-grained ceramic tool for the ultrafine-grained ceramic tool have better thermal stability and bigger hardness. The maximum temperature for ultrafine-grained ceramic tool and common ceramic tool 185 and 168 °C, respectively, and the tool temperature would increase with turning.

(3) Wear behaviors of two kind ceramic tools in turning hardened steels H13 have been studied. The wear depths of common ceramic tool are about many times than which of ultrafine-grained ceramic tool according to the simulation and experimental results. The total wear depths of common ceramic tool are about many times than that of ultrafine-grained ceramic tool. As turning proceeds the amount of wears increases gradually for common ceramic tool and ultrafine-grained ceramic tool.

(4) The experimental results verify primarily the FEM simulation results. The wear depths of common ceramic tool are bigger than that of ultrafine-grained ceramic tool, and there exits scratched marks on the tool flank. The extending directions of wear grooves are different for common ceramic and ultrafine-grained ceramic tool, the former perpendicular to the blade, and the later parallel to the blade of turning tool. The flank wears of tool tip presents grooves generated by abrasive mechanism and adhesion of material which could be due to the abrasive action of hard carbide particles of the work material.

The obtained results provide the fundamental and practical guidelines of the hard turning about the choice of ceramic tool, and the finer grains of ceramic tool can decrease wear.

Acknowledgment This work was supported by National Natural Science Foundation of China (grant No. 50975302).

References

1. Lin HM, Liao YS, Wei CC (2008) Wear behavior in turning high hardness alloy steel by CBN tool. Wear 264:679–684
2. Grzesik W, Zalisz Z (2008) Wear phenomenon in the hard steel machining using ceramic tools. Tribol Int 41:802–812
3. Xie L-J, Schmidta J, Schmidt C, Biesinger F (2005) 2D FEM estimate of tool wear in turning operation. Wear 258:1479–1490
4. Yan H, Hua J, Shivpuri R (2007) Flow stress of AISI H13 die steel in hard machining. Mater Des 28(1):272–277
5. Liu CR, Guo YB (2000) Finite element analysis of the effect of sequential cuts and tool chip friction on residual stresses in a machined layer. Int J Mech Sci 48:1069–1086

6. Fang S, Zhanqiang L, Yi W, Zhenyu S (2010) Finite element simulation of machining of Ti–6Al–4V alloy with thermodynamically constitutive equation. Int J Adv Manuf Technol 49:431–439
7. Lorentzon J, Jarvstra N (2008) Modeling tool wear in cemented-carbide machining alloy 718. Int J Mach Tool Manuf 48:1072–1080
8. Umbrello D, Filice L, Rizzuti S, Micari F, Settineri L (2007) On the effectiveness of finite element simulation of orthogonal cutting with particular reference to temperature prediction. J Mater Process Technol 189:284–291
9. Attanasio A, Ceretti E, Rizzuti S, Umbrello D, Micari F (2008) 3D finite element analysis of tool wear in machining. CIRP Ann Manuf Technol 57:61–64
10. Li JL, Jing LL, Chen M (2009) An FEM study on residual stresses induced by high-speed end-milling of hardened steel SKD11. J Mater Process Technol 209:4515–4520
11. Coelho RT, Ng E-G, Elbestawi MA (2007) Tool wear when turning hardened AISI 4340 with coated PCBN tools using finishing cutting conditions. Int J Mach Tool Manuf 47:263–272
12. Umbrello D (2008) Finite element simulation of conventional and high speed machining of Ti6Al4V alloy. J Mater Process Technol 196:79–87
13. Storch B, Zawada-Tomkiewicz A (2012) Distribution of unit forces on the tool edge rounding in the case of finishing turning. Int J Adv Manuf Technol 60:453–461
14. Calamaz M, Coupard D, Nouari M, Girot F (2011) Numerical analysis of chip formation and shear localization processes in machining the Ti-6Al-4V titanium alloy. Int J Adv Manuf Technol 52:887–895
15. Özel T, Zeren E (2007) Finite element modeling the influence of edge roundness on the stress and temperature fields induced by high-speed machining. Int J Adv Manuf Technol 35:255–267
16. Thakur DG, Ramamoorthy B (2012) Effect of cutting parameters on the degree of work hardening and tool life during high-speed machining of Inconel 718. Int J Adv Manuf Technol 59:483–489
17. Ozel T, Karpat Y, Figueira L, Davim JP (2007) Modelling of surface finish and tool flank wear in turning of AISI D2 steel with ceramic wiper inserts. J Mater Process Technol 189:192–198
18. Wang M, Wang J (2012) CHMM for tool condition monitoring and remaining useful life prediction. Int J Adv Manuf Technol 59:463–471
19. Thamizhmnaii S, Bin Omar B, Saparudin S, Hasan S (2008) Tool flank wear analyses on martensitic stainless steel by turning. Archives of. Mater Sci Eng 32:41–44
20. Afazov SM, Ratchev SM, Segal J (2012) Prediction and experimental validation of micro-milling cutting forces of AISI H13 steel at hardness between 35 and 60 HRC. Int J Adv Manuf Technol 62:887–899
21. Aliakbari E, Baseri H (2012) Optimization of machining parameters in rotary EDM process by using the Taguchi method. Int J Adv Manuf Technol 62:1041–1053
22. Tang ZT, Liu ZQ, Pan YZ, Wan Y, Ai X (2009) The influence of tool flank wear on residual stresses induced by milling aluminum alloy. J Mater Process Technol 209:4502–4508
23. Sun H, Wan N, Chang Z, Mo R (2011) Approach to optimization of part machining service combination. Int J Adv Manuf Technol 56:767–776